On-the-Skin Glucose Sensing and Drug Delivery

Clarence Chan
Jinhong Kim
Celine Ledesma
Qingyuan Liu
Hanyang Zhao

ECE 481 – Nanotechnology
Department of Electrical and Computer Engineering
University of Illinois at Urbana-Champaign
May 13, 2016

Proposal Summary

Given the worldwide occurrence of diabetes and its impact on the daily lives of those who are affected, it is important to address this problem, specifically the need for self-injection of insulin. Currently, insulin is still injected using a hypodermic needle. But before insulin can be injected, the user must regularly monitor his insulin levels typically through the blood glucose level in the form of a finger prick. Here we propose a daily patch that interfaces the drug delivery and the glucose sensor in one package. It is divided into five parts, microneedles, the glucose sensor, insulin storage, device integration, and the battery. The primary focus is on delivering insulin however, it can be adapted for other drug uses as well. The combination of sensing and drug delivery in a discreet and convenient way for users can help change the lives of many.

One of the primary components of the insulin patch are the microneedles. This array of microneedles through which the insulin is released into the body is non-invasive and would not irritate the user. They may also be easily mass produced through standard photolithography, etching, and deposition techniques.

The second primary component is the glucose sensor. The sensor measures glucose levels through the sweat using a graphene with a gold mesh. The Au doped graphene enhances the electrochemical and biochemical activity. There is also a humidity, pH, and tremor sensor used to increase the glucose sensor performance. All these parts work together to provide accurate real-time feedback to the user about his glucose level to his smart phone or portable device.
‘

The insulin is stored in hydrogel which has good biocompatibility and is capable of storing large amounts of liquid. It is proposed that there be three different hydrogels available for different users. For type I diabetics, poly-ethylene-glycol (PEG) is the best option because it can store more insulin whereas type II diabetics should use PNIPAAm because they provide a faster response. For mild diabetics, a solution-like hydrogel is the easiest and cheapest option.

The way all these functions would be powered would be through a flexible and stretchable battery. This battery is composed of carbon nanotube electrodes and a nanoporous anodic aluminum oxide as the dielectric. This battery has a high capacity and has a solid dielectric to avoid leakage. The battery has a serpentine design and is bonded to a silicone substrate which allows it to stretch and flex without breaking.

Integrating all of these devices is a feedback loop that dictates when insulin should be released and how much. This includes the piezoelectric mechanism that controls when the hydrogel is in contact with the microneedle array. Lastly, all the components would be bonded to a silicone substrate and the devices that are not thin enough would be placed inside a microfluidic enclosure.

Table of Contents

I. **Micro-needle fabrication and integration**

II. **Sweat sensor based on graphene to manage diabetes through the skin**

III. **Hydrogel drug delivery**

IV. **Stretchable capacitor and fabrication**

V. **Glucose feedback loop, inverse piezoelectric control mechanism and system integration**

VI. **References**

VII. **Budget proposal**

I. Micro-needle fabrication and integration

A key aspect to drug delivery in biomedical wearable devices is the necessity of un-intrusive treatment. Such systems must not only be void of irritation for the user, but also be unobtrusive in physical form. As per the requirements of insulin administration, a needle-based injection system is proposed. In order to avoid the obstructive and irritation prone nature of conventional hypodermic needles, the injection system will employ micro-needles (MNs) to minimize the aforementioned effects on the user.

The implementation of MNs as a method of drug delivery has been realized via existing microfabrication techniques as early as mid-1990's. Such needles are generally polymer, Si, metal, glass or ceramic based microstructures with a diverse range of structural variations **[1]**. **Fig. 1** depicts several methods of drug administration with different forms of MNs.

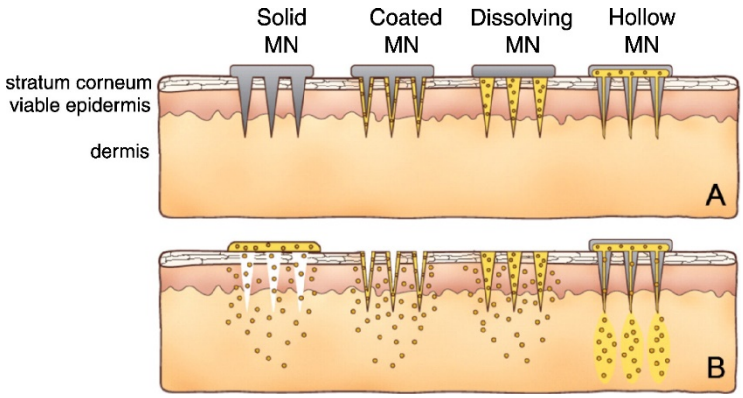

Fig. 1a) Various micro-needle systems applied to the skin and **b)** the associated drug delivery mechanism of each corresponding micro-

In the case of the proposed medical device the hollow MN is adopted for its re-usability over single dose systems such as the solid, coated and dissolving mechanisms. While well-developed fabrication techniques for each material and type of MN exist, the proposed device will utilize a hybrid form of MNs composed of Si and Si_3N_4 for ease of fabrication, reliability and consistency in concordance with industrial level wafer processing techniques from etching to deposition methods.

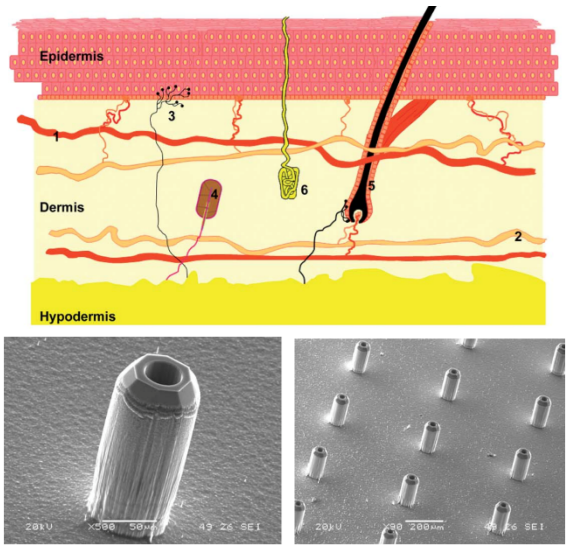

Fig. 2a) Cross sectional diagram of skin layers including nerves and internal components of dermis layer **[2]** and **b)** A hollow MN structure with length of 200µm and hole diameter of 30µm **[4]**.

Although MNs are simplistic in form, care in design must be taken to ensure performance. In order to effectively administer insulin for a user, the needles must be capable of penetrating the outermost layer of the skin, the stratum corneum, or SC (see **Fig. 1a**). It has been suggested that the length of MN structures should be kept around 200µm to avoid contact with nerve endings situated in the dermis (see **Fig. 2a**) Error! Reference source not found.. Despite this however, different physical lengths ranging from 150µm **[1]** to 350µm **[3]** have been demonstrated in Si. Other design parameters include MN hole diameter which was suggested to be on the order of ~30µm (see **Fig. 2b**) to prevent blockage by red blood cells, cited as 20µm in diameter **[4]**. Additionally, is the consideration of adverse health effects to the user with a punctured SC layer, which traditionally acts as a natural blocking layer to pathogens and foreign substances. While it is known that bacterium such as *E. Coli* is capable of

penetrating the skin, it is also shown that the level of bacterium access to the body is no greater than a conventional hypodermic needle **[5]** if not less **[6]**. At the same time, it has been shown that skin recovery in terms of the basic barrier layer after penetration by MN arrays (MN length of 150µm) is relatively fast, at around 2 hours without occlusion of punctured areas **[7]**.

With the considerations discussed, the proposed MN array will consist of microstructures with a length of 200µm, MN diameter of 70µm, MN hole diameter of 30µm and pitch of 220µm. While the MNs will be pillar shaped instead of pyramidal, holes will be drilled off-center such that the pointed tips of each MN can be preserved thus maximizing penetration capability while minimizing blockage probability **[3]**.

A standard single crystal Si wafer is used to begin fabrication of the MN microstructures. In order to obtain the desired point on the MN tip, a directional etch is performed on the Si substrate using a standard KOH solution to create inverted pyramid structures (see **Fig. 3c**) **[8]**, note pattern sizes may have to be pre-defined with lithographic techniques to adjust pyramid base diameter **[9]**.

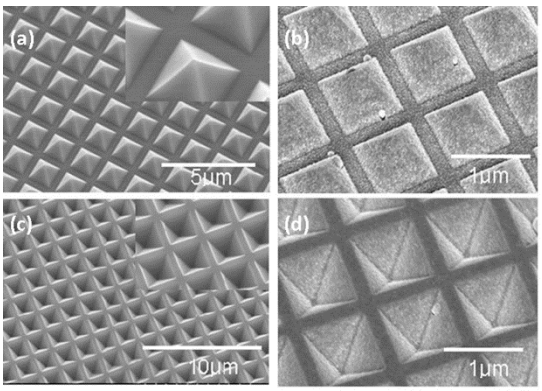

Fig. 3a) Positive pyramids replica, **b)** positive pyramids replica with 200-nm thick gold deposited, **c)** inverted pyramids replica and **d)** inverted pyramids replica with 200-nm thick gold deposited **[8]**.

Next, a thin layer (10 nm) of sacrificial SiO_2 is first deposited via LPCVD onto the ordered inverted pyramid array. Following this, a layer of Si_3N_4 is deposited also via LPCVD with a thickness greater than 200µm to account for the target MN length. This is done over PECVD as it has been reported that Si_3N_4 deposited through LPCVD has greater resistance to HF and BHF solutions than those deposited with PECVD **[10]**.

Once the three layer stack of substrate Si, SiO_2 and Si_3N_4 have been deposited, an additional layer of epitaxial Si is grown atop of the amorphous nitride layer **[11]** as a backside layer to the MN array. The final structure as we have described to point is shown in **Fig. 4**.

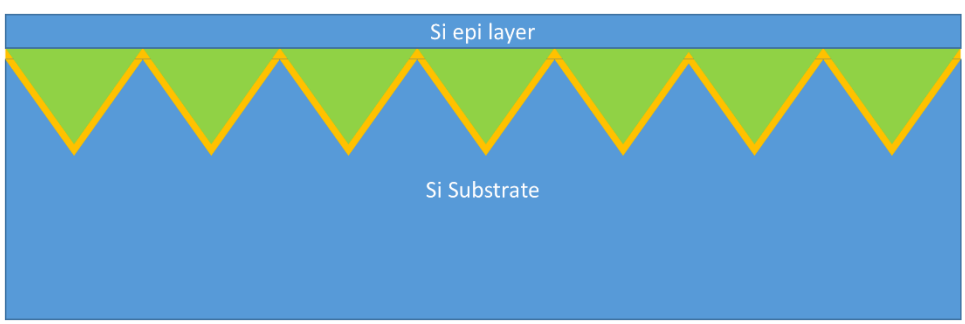

Fig. 4 Cross sectional view of stack structure with Si substrate (blue), SiO_2 sacrificial layer (orange), Si_3N_4 pyramid structures (green) and an additional MN array backside Si epi layer.

The same KOH etching procedure could then be repeated to form smaller off-center pyramids in the Si epi layer. This is to act as a funnel structure which will allow enhanced drug collection for the MN hole which will be processed in a later step. It should be noted that the 'funnel' diameter, i.e. the pyramid base should be of smaller diameter to the target diameter of each MN structure (around 40µm instead) such that it is situated within the final MN. This structure is shown on the following page in **Fig. 5**. Once

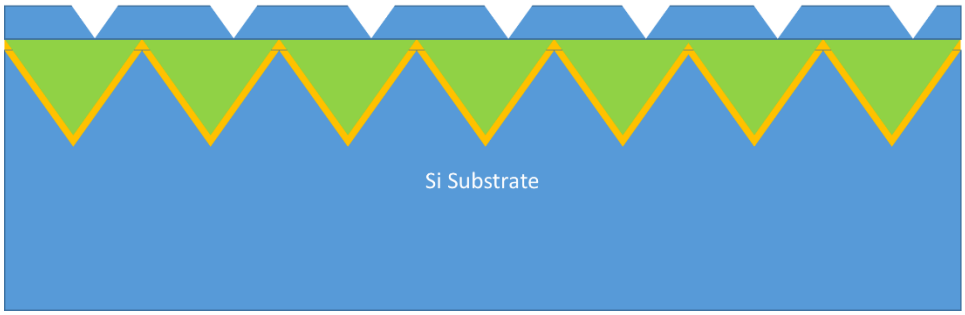

Fig. 5 Cross sectional view of stack structure with Si substrate (blue), SiO_2 sacrificial layer (orange), Si_3N_4 pyramid structures (green) and directionally etched array in Si epi layer.

this final structure has been fabricated, it is now possible to 'lift off' the pyramidal stack from the original Si substrate by selectively etching the SiO_2 sacrificial layer using 5:1 BHF, leaving an array of Si_3N_4 pyramid microstructures shown in **Fig. 6**. Re-use of the original Si substrate as a mold for new pyramidal arrays may be possible depending on damage from chemical etching.

Fig. 6 Cross sectional view of Si_3N_4 microstructures with patterned Si epi layer backside.

With the structure depicted in **Fig. 6**, it is possible to fabricate needle structures first by spin casting the array with a resin such as PMMA to planarize the uneven surface. This can then be patterned using a standard lithographic mask. Cr could then be deposited over the planar surface and lifted off with PMMA development as shown in **Fig. 7a**, yielding caps of PMMA coated with Cr. The final needle structure can then be produced by a two-step dry etching process. The first is a modified RIE method to selectively etch away previously defined portions of Si_3N_4 **[12]** down to the Si substrate as depicted in **Fig. 7b**. Once this is achieved, a second resin must be spin-casted again on the needles such that the Cr mask may be patterned for MN holes and channels are then etched through the Bosch process with DRIE **Fig. 7c**, with the PMMA and Cr mask removed as shown in **Fig. 7d**.

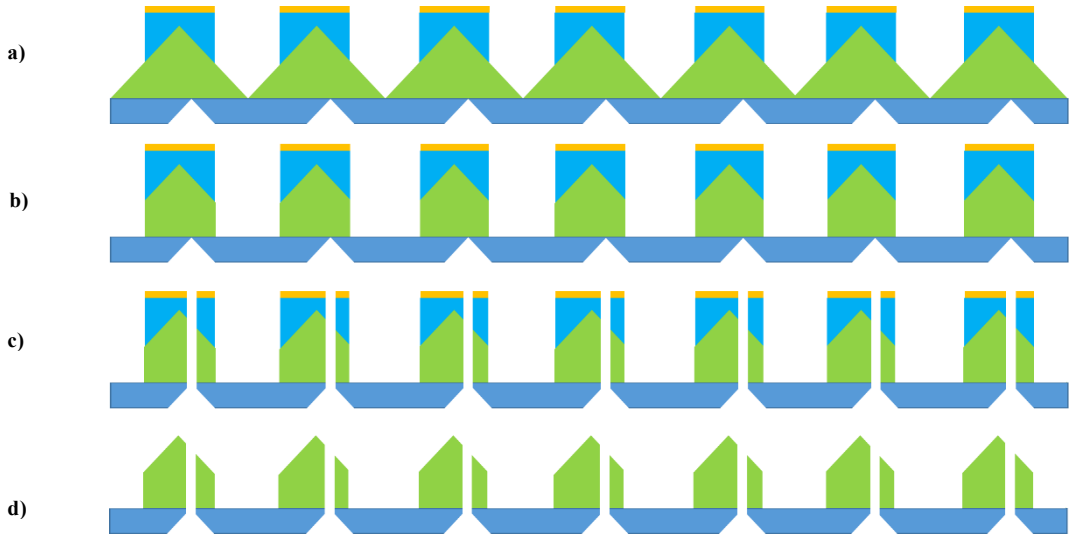

Fig. 7a) Cross sectional view of Si_3N_4 microstructures with patterned PMMA and Cr coating **b)** selective removal of Si_3N_4, **c)** patterning of Cr coating and DRIE of MN holes and **d)** finalized MN array with PMMA coating and Cr lifted off.

Drug delivery will be enabled through a hydrogel containment layer mounted above each MN. In order to allow electrical actuation and controllability of the drug to needle delivery, additional processing to the finalized MN structure is required. The mechanism proposed is the addition of a patterned piezoelectric mesh layer on the Si backside of the MN array which will allow electrical interfacing to raise or lower the hydrogel drug containment and place it in contact with the MNs when administration is required. PVDF is proposed as the piezoelectric material to allow the described mechanism to function. A cross sectional view of this mechanism with an associated hydrogel layer is shown in **Fig. 8**.

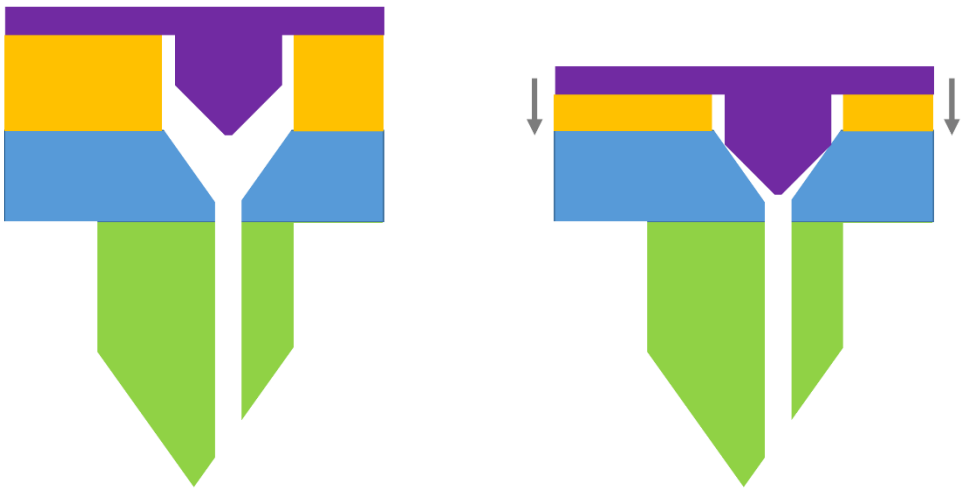

Fig. 8 Cross sectional view of PVDF piezoelectric elements (orange) in relaxed and contracted state, moving hydrogel element (purple) into contact with Si funnel.

With the integration of electronic control, a positive or negative bias can be applied to expand or contract the piezoelectric supports which would allow for drug diffusion from its hydrogel containment to the prefabricated MNs, with scaling done on a wafer level. The scalability and relative simplicity of the MN design and fabrication procedure described in this section is highly beneficial in mass producing low cost arrays for drug delivery that could be extended beyond the proposed target of insulin administration. Similarly, the hydrogel layer of the device could also be molded and produced in the same array-like fashion meaning overall device scalability is possible. The hydrogel containment system will be discussed in detail in the following section and the electrical feedback and actuation is also discussed in a later portion of the proposal.

II. Sweat sensor based on graphene to manage diabetes through the skin

The global increase in diabetes is a significant physical and economic problem. Reducing the morbidity of the disease requires the effective control of glucose levels through the diet and drug treatment such as insulin injections. The insertion sensor under the skin and finger stick, a finger is pricked with a lancet to obtain a small quantity of blood for testing, have been used to monitor the glucose levels. However, these procedure only monitoring glucose level produce poor results such as overdose of drugs. Graphene is an excellent material in micro- and nanotechnology due to its conductivity, high carrier mobility, flexibility and optical transparency **[13]**. In addition, biocompatibility of graphene is a promising candidate for healthcare applications; however, it has limited uses in electrochemical devices for the detection of pH **[14]**, ions **[15]** and biomolecules **[16, 17]**. In this proposal, improved sweat sensor based on graphene through the skin is presented for accurate monitoring diabetes. The skin-mounted graphene-hybrid device is capable of monitoring glucose level and pH and the estimated levels of glucose in the blood can be determined by measurement of sweat glucose concentration **[18]**. The continuous point-of-care monitoring of bio device based on electrochemical sensing provide unique solutions for the treatment of diabetes **[13]**. The point-of-care treatment of diabetes would be realized when the connection of GP-hybrid wearable devices to a portable and wireless power supply.

The device array fabrication starts with the spin-coating of the epoxy layer which thickness is ~1.5um on a nickel sacrificial layer using thermal evaporation deposited on the silicon wafer. The bottom epoxy layer is patterned by photolithography. Thin film of Cr/Au is formed ~7nm/~70nm respectively using thermal evaporation and patterned as the Au mech interconnects using photolithography and wet etching [13]. The graphene synthesized by the CVD is transferred and patterned. The device is finally encapsulated with another epoxy layer and transferred onto a PDMS substrate after eliminating a nickel sacrificial layer as shown in **Fig. 1**. **Fig. 1** a) presents the schematic and corresponding images of the GP-hybrid electrochemical device. The sweat control components (i, ii) consists of a sweat-uptake layer and waterproof film and sensing components (iii–vii) are composed of humidity, glucose, pH and tremor sensor as shown in **Fig. 1**. High conductivity and mechanical reliability for stable electrical signal transfer is performed by the bilayer structure; top of Au serpentine mesh sheet and gold-doped graphene sheet at the bottom. The serpentine Au mesh subjacent to gold-doped CVD graphene enhances the electrical conductivity in comparison with conventional transparent electrodes. The serpentine structure Au mesh also enhances both the conductivity and mechanical deformability. Figure 4 h, i show the relative resistance changes of the electrode under applied strain up to ~30% and this graph shows the sensor is stable against compressed and stretched strain. Gold-doped graphene of sensor enhances the electrochemical activity and biochemical sensitivity. In contrast to conventional electrochemical sensing, Ag/AgCl counter electrodes provide portability and wearability of the electrochemical system. **Fig. 3** indicate the schematic illustration of sweat control, glucose, pH and tremor sensing to explain the process of the diabetes monitoring.

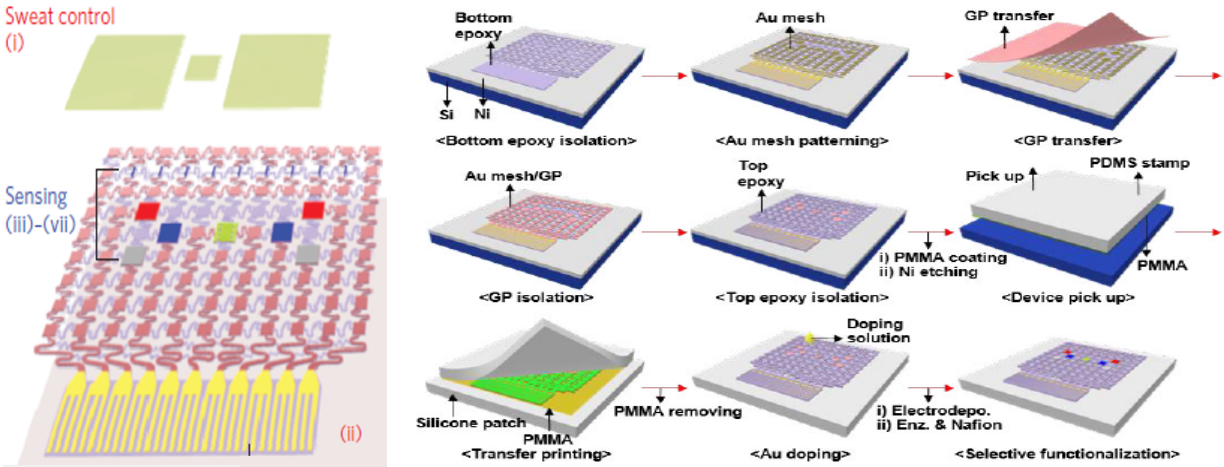

Fig. 1. a) Schematic illustration of GP-hybrid electrochemical device, **b)** Schematic illustration of the fabrication process of the graphene-hybrid electrochemical sensor **[13]**

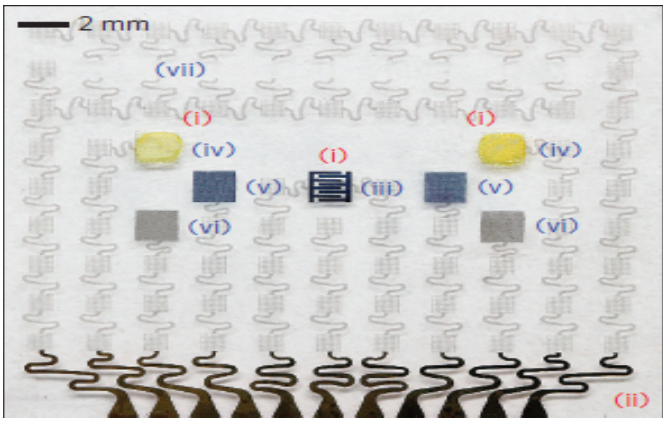

Fig. 2. Images of the GP-hybrid electrochemical device corresponding to illustration of **Fig. 1**. (i) sweat-uptake layer (Nafion); (ii) water-proof film (silicone); (iii) humidity sensor (PEDOT); (iv) glucose sensor (PB); (v) pH sensor (PANi); (vi) counter electrode (Ag/AgCl); (vii) tremor sensor (graphene) **[13]**

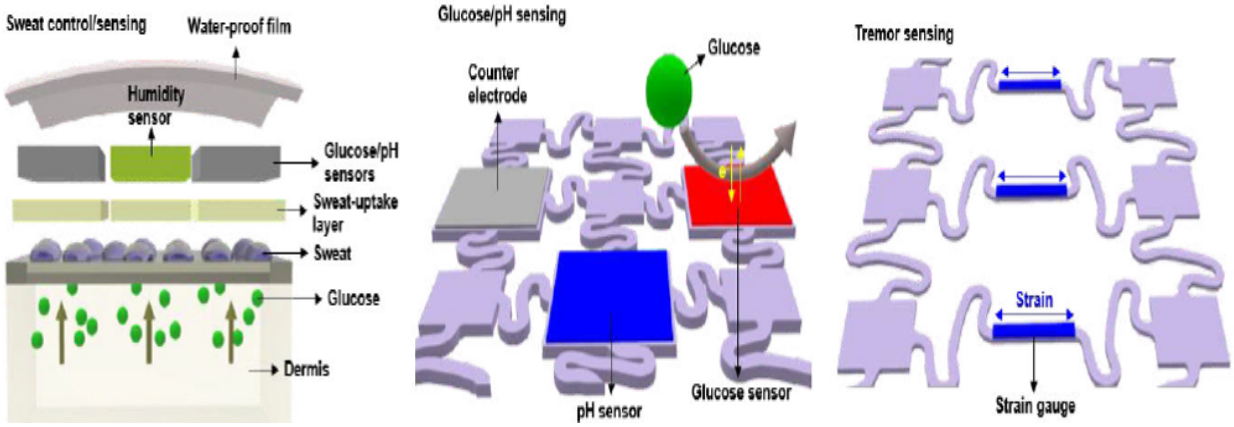

Fig. 3. Operation process of the diabetes monitoring using patch; sweat controlling, Glucose, pH, tremor sensing **[13]**

Sensitivity of the glucose sensor with glucose oxidase is affected by environmental conditions such as pH, temperature, oxygen level and glucose on the skin. The humidity sensor monitors Relative Humidity (RH) and determines the starting point of glucose and pH sensing when RH value is above than

80%. The different pH effect to the glucose sensor is estimated by relative current changes of the glucose sensor as shown in **Fig. 4a**. The **Fig. 4b** presents the temperature dependency of the glucose sensor. The sensitivity is slightly decreased as the temperature decreases while the sensitivity of the pH sensor is constant at various temperatures in figure 4c. The effect of oxygen level in the blood should be counted to increase the sensitivity of glucose sensors based on the glucose oxidase. Inconstancy of oxygen levels causes to overestimate or underestimate glucose levels. The glucose level in the patch is contacted with the air where the amount of oxygen is much larger than that in the blood and sweat. Thus, the glucose sensor is also measured under the air condition and the influence on the glucose oxidase would be minimal. Even though the glucose in the outer layer of skin could be related to measure the glucose lever, its amount is not large enough to affect the sweat glucose sensing **[19]**. Figure 4d shows sweat glucose concentrations without considering the glucose in outer layer of skin and the graph indicates an excellent linear correlation with glucose concentrations. Therefore, additional warm-up period to generate sweat is not necessary to measure the glucose level using patch. Small P value shows that the results are statistically reliable due to the statistical analysis between the sweat glucose concentration measured by patch and commercial glucose assay.

The diabetes patch needs at least 20ul of human sweat for measurement of the glucose concentration. No disturbance is found in larger volumes of sweat as shown in **Fig. 4 e, f**. The figure 4 g. indicates that the high concentration of glucose is successfully detected; however, the glucose sensor is susceptible to error due to pH changes (blue). Therefore, glucose monitoring with real-time correction of pH measurement (red) is necessary to increase the reliability of sensor. In hypoglycaemic states, where physiological tremors occurs with a frequency over 1Hz, the tremor sensor in the patch detects the small tremor and it also results in increased stability of sensor.

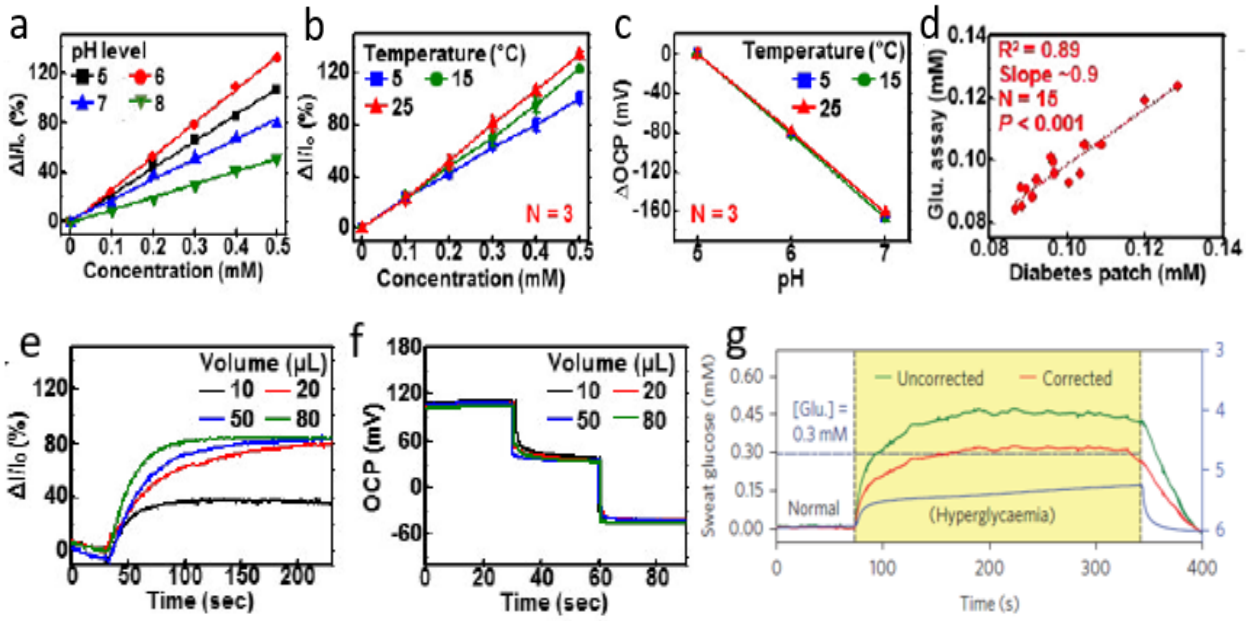

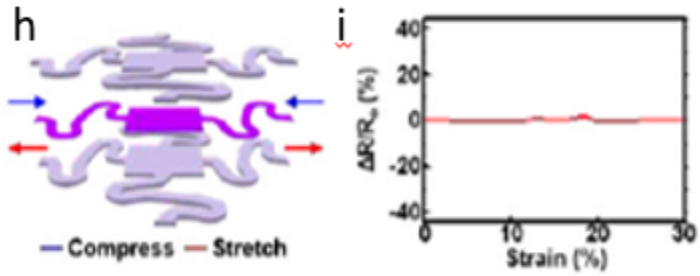

Fig. 4. **a)** pH dependency of the glucose sensor; relative current changes of the glucose sensor at different pH level, **b)** Plotting of the glucose sensor at different temperature, **c)** Circuit potential changes of pH sensor at various temperature, **d)** Calibration plots of the correlation between the sweat glucose level measured by the patch and that measured by the commercial glucose assay; small P value approaches more reliable, **e)** Effect of sweat amount on the glucose sensor, **f)** Influence of sweat amount on the pH sensor, **g)** Calibration curves of glucose and pH changes under artificial sweat, **h)** Schematic illustration of Au mesh and graphene bilayer electrode, **i)** Curve of relative resistance under applied strains up to ~30%.

In this proposal, we suggest improving the glucose measurement by sweat sensor based on graphene with Au mesh for diabetes since gold-doped graphene of sensor enhances the electrochemical activity and biochemical sensitivity. The glucose concentration from the skin can be more accurately measured by adding humidity, pH sensor and tremor sensor with glucose sensor. The bilayer fabrication structure such as top of Au serpentine mesh sheet and gold-doped graphene sheet at the bottom has advantage to enhance the device performance by increasing conductivity and mechanical reliability for stable electrical signal transfer. The serpentine structure of Au mesh also enhances both the conductivity and mechanical deformability. The counter electrode of Ag/AgCl provide portability and wearability of the electrochemical system. These advanced patch provide new opportunity for the treatment of diabetes by measuring real-time correction of glucose level using smart phone and portable device.

III. Hydrogel drug delivery

Hydrogel drug delivery method is gaining its popularity through years. Hydrogel, by definition, is a polymeric materials, the hydrophilic structure of which renders them capable of holding large amounts of water in their three-dimensional networks **[20]**. It is shown that a lot of hydrogel have a very good biocompatibility **[21, 22]** as it would not trigger any, or extremely low amount of biological irritation or immune response. Therefore, with the method of trapping drug molecules under hydrogel, it provides a controlled diffusion mannered drug delivery method.

A lot of polymeric hydrogel material is available by varying its polymer length or copolymers ratio. A very interesting hydrogel polymer material named poly(N-isopropyl-acrylamide) (PNIPAAm), a temperature sensitive hydrogel **[23]**, could be used for insulin delivery. Based on requirements, comonomer butyl methacrylate (BMA) is introduced into N-isopropyl-acrylamide (NIPAAm) gel to increase their mechanical strength **[23]**. Molecular structure of PNIPAAm and PNIPAAm copolymerize with BMA is shown in **Fig. 1**. PNIPAAm hydrogel has a negatively thermosensitive drug release system, undergoes reversible lower critical solution temperature (LCST) phase transition. As the environment is above 32°C, the gel shrinks to a dehydrated state. Normally, gel will absorb more water in as temperature increased. The reversible LCST can be tuned by modify the PNIPAAm hydrogel with additional hydrophilic monomer to increase reversible LCST or introduce more hydrophobic monomer to decrease reversible LCST.

Utilizing a temperature sensitive hydrogel would allow the delivery not only just depends on concentration drugs retained in hydrogel but also allows us to squeeze the drug out with respect to temperature difference, by on-off release mechanism, show in **Fig. 2**. As there is temperature difference between epidermis layer and dermis layer, the further it travelled through the skin, the higher temperature it will have **[24]**. In this proposal, we could tune the delivery rate not only by how much area hydrogel is in contact with the dermis tissue but also how far it penetrated. Furthermore, on-off release system is relatively faster comparing to diffusion system.

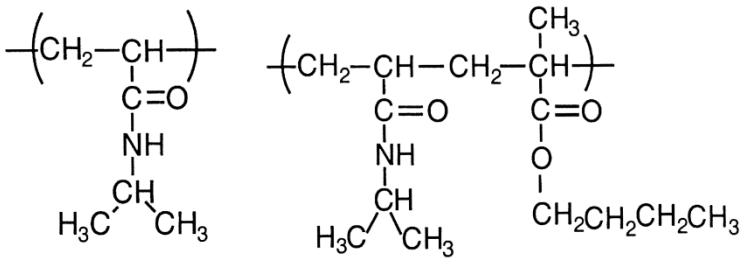

Fig. 1 The left molecular structure is for poly(N-isopropyl-acrylamide) PNIPAAm; Molecular structure on the right is for poly(NIPAAm-co-BMA)

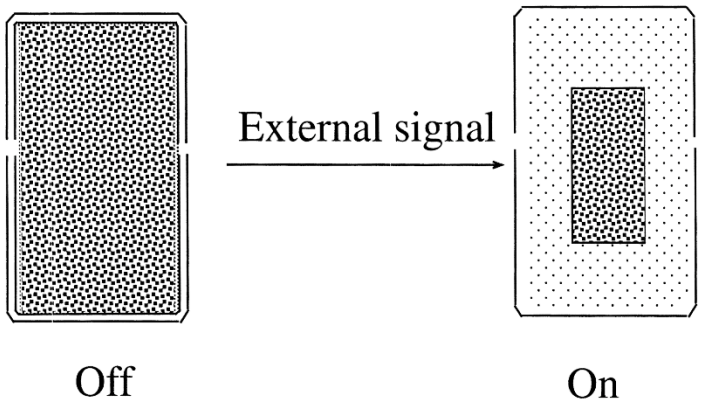

Fig. 2 Schematic illustration of on-off release from a squeezing hydrogel device for drug delivery **[23]**

For loading the insulin drugs to the hydrogel, a very common approach would be freeze drying the hydrogel in order to create porous microstructure that allows drug solution to first diffuse into the gel and contained by the structure. The hydrogel structure after freeze drying is shown in **Fig. 3**.

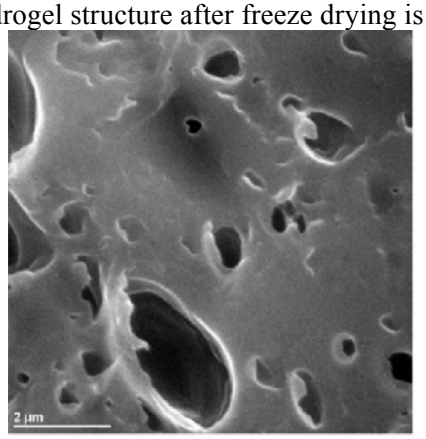

Fig. 3 SEM micrographs of freeze-dried PNIPAAm hydrogel **[25]**

From literature **[26]**, it is shown that it is possible to manufacture a patterned PNIPAAm brushes on silica surface by microcontact printing followed by surface-initiated polymerization. The method uses a silicon (111) wafer as a substrate and starts with microcontact printing of alkyl-trichlorosilane-based self-assembled monolayers (SAMs) of octadecyltrichlorosilane (OTS). A solution of OTS in hexane is then linked onto a polydimethylsiloxane (PDMS) stamp. After that, wafer is backfilled with 3-(Aminopropyl) triethyxysilane (APS) and initiated the polymerization of NIPAAm using NIPAAm, CuBr, pentamethyldiethylenetriamine (PMDETA) and methanol/water. The schematic procedure is illustrated by **Fig. 4**.

This patterning technique allows the possibility of different number of PNIPAAm brushes per area. This gives us an additional way to control the drug delivery rate by the amount of hydrogel is available in contact area for drug delivery.

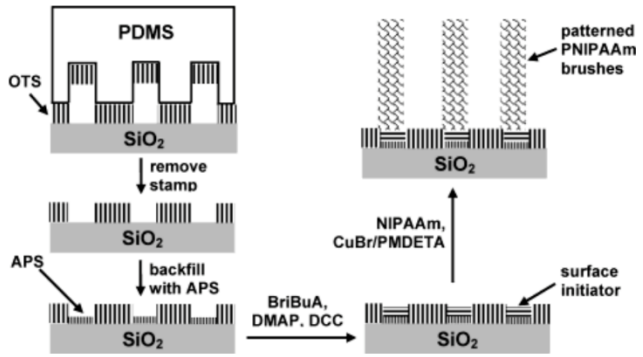

Fig. 4 Schematic procedure for micropatterning of PNIPAAm brushes on silica substrates **[26]**

With all the advantages of using PNIPAAm hydrogel, that allows controlling of the delivery by depth of hydrogel penetrate, different area to diffuse, additionally with fast drug release system, however, with a major limitation is that there is not much study being done towards cytotoxicity, carcinogenic or teratogenic of PNIPAAm. Study shows acrylamide-based polymers activate platelet upon contact with blood **[23]** alerted that PNIPAAm requires extensive study towards its biocompatibility. Additionally, the drug is diffused into hydrogel, drug load is limited by diffusion and porosity after freeze-drying.

Other than using PNIPAAm hydrogel as the drug container, choosing a well-studied hydrogel with great compatibility **[27]** such as poly-ethylene-glycol (PEG) can be used instead. Figure 5:

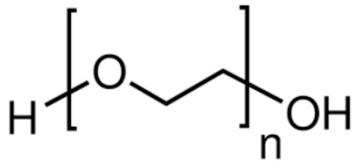

Fig. 5 Molecular structure of poly ethylene glycol (PEG)

Besides using freeze-drying method to load insulin into the gel, PEG hydrogel can be patterned by maskless stereophotolithography (SLA) (3D printing) using polymerization of a crosslinkable polymer solution immediately after printing onto a substrate. Various technique of fabricating 3D PEG hydrogel is proposed and a standard experimental set up is illustrated via **Fig. 6a**. **[28]**. **Fig. 6b** illustrates the scaffold image of PEG. This method works with various hydrogel material, however, there is no literature showing that this method can be worked with PNIPAAm. This fabrication method allows drug solution directly transferred to the hollow space acting as a drug reservoir of the hydrogel, with no limit of the porosity; no diffusion is required of letting drug solution get absorbed by hydrogel. This allows a lot more drug load to the hydrogel, a relatively concealed environment for the drugs.

Though maskless SLA allows basically any types of surface patterning or shape of hydrogel to be fabricated. However, this bottom up method is slow and expensive. Additionally, utilizing those hydrogel has a relatively slower drug delivery rate as the delivery is controlled by diffusion. However, under a lot of criterion, insulin is needed to spike up quickly as glucose entered into blood stream.

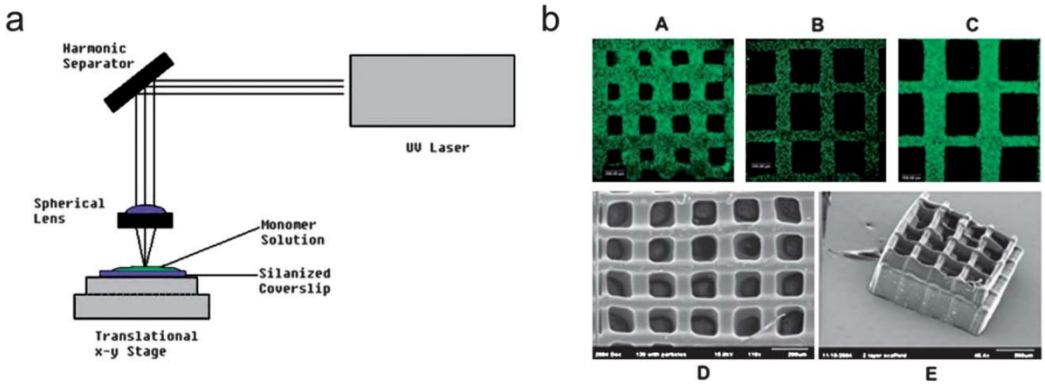

Fig. 6 (a) experimental setup for layerwise stereolithographic fabrication of patterned scaffolds **(b)** (A-C) confocal microscopy images, (D-E) SEM micrographs of PEG scaffold **[28]**

Another kind of hydrogel, similar to PNIPAAm, is thermal-sensitive but would undergo solution-gel phase transition instead of gel swelling-shrinking transitions because there is no cross-linker between each polymer strand **[23]**. As temperature goes higher, the hydrogel becomes solution-like. There are a lot of hydrogels with this property around body temperature commercially available as this property is studied extensively for drug delivery such as Pluronic® , Pluronic® R, Tetronic® and Tetronic® R etc. Those products are mainly constituted of block copolymer of poly(ethylene oxide) (PEO) and poly(propylene oxide) (PPO). A lot of times, poly(lactic acid) (PLA) is introduced to copolymerized with PEO for tuning the LCST as well. Those hydrogel has the perfect biocompatibility and is biodegradable, the amount of insulin that is delivered depends on how much hydrogel is entering into the dermis layer as the hydrogel together with the insulin would dissolved into dermis layer. Loading of insulin to this hydrogel can be accomplished via freeze-drying and diffuse the drugs to the gel.

Using solution-like hydrogel is relatively the easiest hydrogel delivery system among all three choices of hydrogel mentioned in this proposal. As the total amount of drugs that would be delivered to the system is directly related to how much hydrogels go into the system. No diffusion is needed for considering how much drugs would go into the system. However, the rate of delivery would not be as quick comparing to PNIPAAm, and loading of the drugs per hydrogel is depends on diffusion after freeze-drying, drug load can be applied is limited.

For all three choices of hydrogel, different hydrogel can be utilized based on different diabetics condition. For type I diabetics, as not enough insulin is provided, using second hydrogel choice which is PEG with maskless SLA fabrication method is preferred as patient requires large amount insulin. For type II diabetics, where biological system is capable of producing enough insulin, just in a slow time manner, utilizing PNIPAAm is better as it gives a quicker release of the insulin. For mild diabetics, using the third kind of hydrogel which is solution-like as it provides the easiest, probably the cheapest hydrogel choice.

IV. Stretchable capacitor and fabrication

Although not central to the operation of the skin mounted insulin monitor and injector, the battery for the device is still an important part of the whole system. The proposed system is not only a flexible battery but also a stretchable battery which makes the overall device less obtrusive. The battery will also have a high energy capacity to power day long operations but will not require the ability to recharge as the system will only work for one day use.

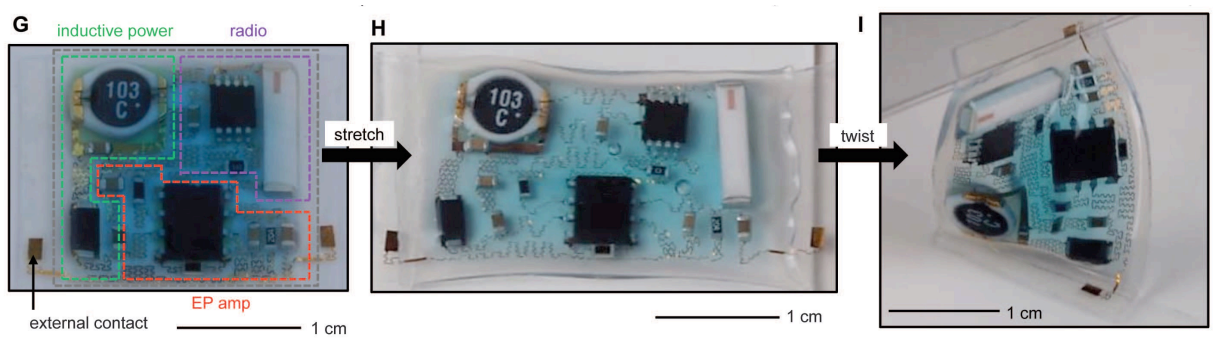

Fig. 1 g) subsections of the circuit in the microfluidic enclosure **h)** microfluidic enclosure when stretched **i)** microfluidic enclosure when twisted **[29]**

There have been a few papers about the development of flexible electronics but the most notable one is the design in 2014 using serpentine interconnects and electronic components suspended in a dielectric fluid, all encapsulated by a polymer substrate shown in **Fig. 1 [29].** The battery is a solid off-the-shelf capacitor. It is notable because it can accommodate up to a 100% strain. However, many of the components do not lie flat against the skin. Furthermore, the silicon encapsulation could be punctured and leak the dielectric fluid. This is still a good option for housing various components, but it would be best to minimize the number and size of components and replacing the power source would make the greatest impact.

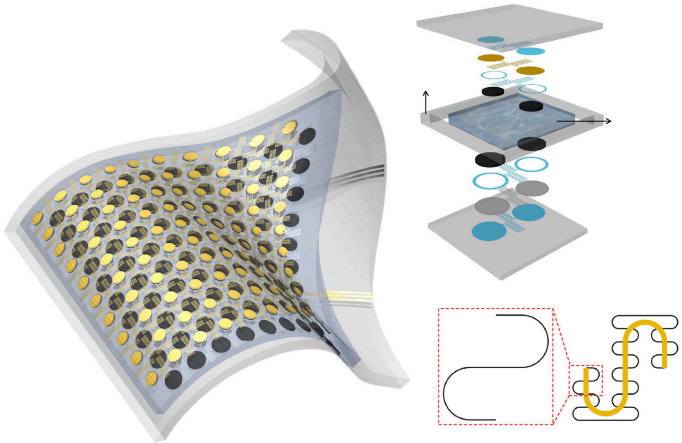

Fig. 2 Electrochemical stretchable battery **[30]**

Another option would be to use a flexible battery also developed by the same group. This battery shown in **Fig. 2** uses a silicone enclosure with an array of bottom and top array of cathodes and anodes sandwiching a gel electrolyte layer. This design can accommodate up to 300% strain and has a capacity density of ~1.1 mAh cm^{-2} **[30]**. Moreover, another capacitor was made using a configuration similar to the serpentine but was not primarily used as a battery. In this skin mounted insulin monitor and injector, the degree of strain the battery can endure is less of a concern as the capacity of the battery. This leads into the possibility of using thin film batteries.

By using a combination of thin film batteries and the interconnect design used in the previously mentioned papers, higher capacity batteries can be integrated into stretchable skin based technology. The battery is based off of research done on using carbon nanotubes (CNT) as the cathode and anode and nanoporous anodic aluminum oxide (AAO) as the dielectric **[31]**. A cutaway for the battery structure is shown in **Fig. 3**. This would be better than using the electrochemical battery because the dielectric wouldn't leak and the lack of need for encapsulation would allow for more complicated designs for the battery. The paper also shows that the carbon nanotube battery has a high energy and power density which is especially useful in devices of limited space such as the one proposed.

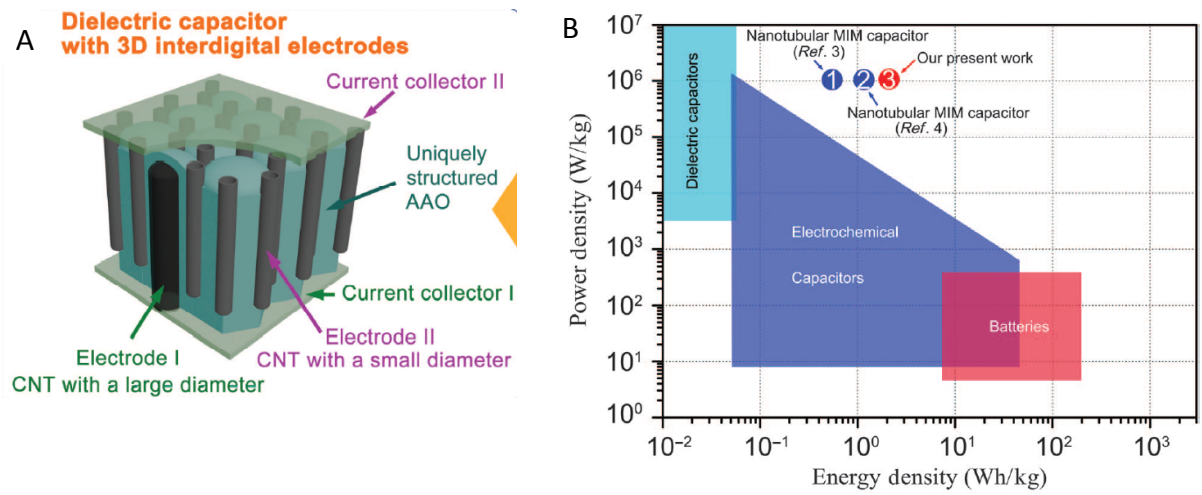

Fig. 3 a) dielectric capacitor with carbon nanotube electrodes **b)** dielectric capacitor showing high energy density and power density **[31]**

The proposed pattern of the design is the half-and-half Peano design in **Fig. 4**. This design allows for strain of up to 16% in the horizontal direction and 13% in the vertical direction **[32]**. Allowing nearly even strain allows for adequate stretching in all directions.

Overall, the proposed battery configuration consists of the CNT and nanoporous AAO battery patterned as in the form of the half-and-half Peano design. This design would allow for a stretchable and high capacity battery which could pave the way towards more functional skin based technology. Furthermore, the functionality of the proposed Peano battery could be increased by adding an inductive coil.

Fig. 4 half-and-half Peano structure **[32]**

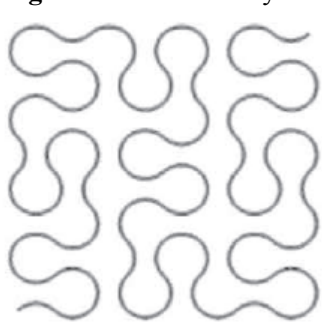

This design can be accomplished by modifying the fabrication procedure of the CNT and nanoporous AAO battery and electrochemical stretchable battery with wireless charging. First the nanoporous AAO membrane must be made. A general overview of this process is shown in **Fig. 5**. This is done by taking high purity Al foil and anodizing it in oxalic acid solution, this forms the AAO membrane which is then removed. The AAO membrane goes through hard and current anodization. The hard anodization forms MA-AAO which eventually houses the larger central CNT and current anodization forms the hexagonal CNT array around the larger CNT. The last step is etching the hexagonal array all the way through the capacitor **[31]**. A more detailed description of the process can be found in the original publication.

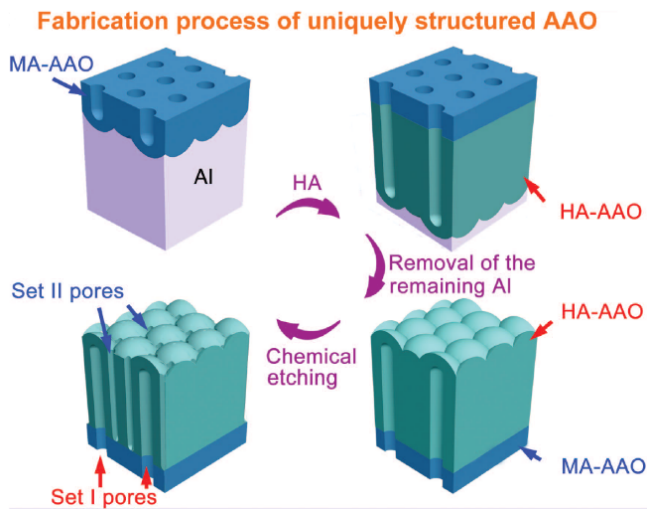

Fig. 5 fabrication process of the AAO dielectric [31]

Afterwards, the membrane would be attached onto a silicon substrate and using photolithography and reactive ion etching, the Peano design can be etched all the way through the capacitor. The CNTs will be grown by placing the AAO membrane into a tube furnace through pyrolysis of acetylene. If there is time, it would be interesting to see if it is possible to remove the carbon nanotubes from the AAO matrix as it would result in CNTs of equal length and a specific diameter. This could be done by continuing to etch away the AAO matrix.

After the creation of the CNTs, both sides of the Peano battery will be have Au sputtered onto it. Finally the battery will be transferred onto the silicone substrate, attached to the necessary components, and then encapsulated. The resulting device would then be able to serve as the power supply for the piezoelectrics as well as the chip and sensors that monitor and inject the insulin.

V. Glucose feedback loop, inverse piezoelectric control mechanism and system integration

Diabetes or diabetes mellitus is one of the most common disease in the world, about 415 million people is suffering from it by 2015 **[33]**. There are meanly three types of diabetes by different mechanism. In short, type 1 diabetes patients cannot produce insulin or enough insulin by themselves, and type 2 diabetes patient's targeting cells are unable to response to insulin, gestational diabetes is when pregnant women experiencing high blood sugar level without diabetes history. Here only type 1 and type 2 will be discussed.

If a patient doesn't keep his or her glucose in blood within a certain level, there will be many potential complications. One effective treatment would be take in insulin from outside source. Traditionally a patient need to monitor his or her glucose level in blood by taking blood from thumb and test it, with the result they need to inject insulin by needle manually. This method is not only painful but also wearing. What we proposed here is a smart patch which will detect glucose level from sweat, track food take in and automatically release certain amount of insulin to maintain the right glucose level.

In this part of the proposal, glucose feedback loop, Inverse piezoelectric control mechanism and system integration will be discussed.

1. Glucose feedback loop

This will be a discrete time interval close loop feedback system with one sensor and two input method, aiming to stabilize the glucose level in blood. The sensor will be the sweat glucose detector integrated into the patch and will report data every 10-20 minutes, the data from the sweat usually have a 15-20minute lag from the real value in the blood.

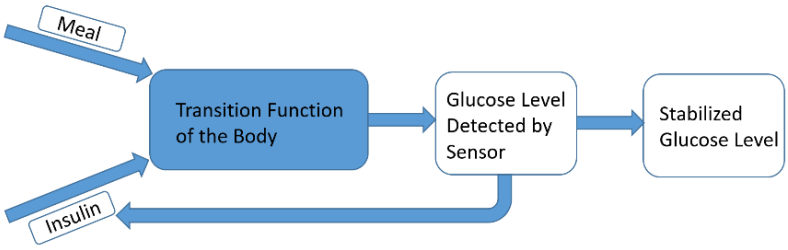

Fig.1 The close loop feedback system diagram

One input, or set of inputs will be the food take into the body which will be manually input by the user on their smartphone. These inputs will include the start and end time of the meal, the composition and weight of the meal. There will be data preset for majority food provider, for example Subway and McDonalds, so the user won't need to worry about memorizing all these. There will also be user customized menu for user cook regular meal at home. Another input is the insulin release rate which is controlled by inverse piezoelectric control mechanism. The insulin will help control the glucose level down to an expected level. One possible input is connected sports tracking device or smart watch, because sports can change the glucose level in blood dramatically, but these functions will not be integrated in the patch.

The transition function, which will convert the inputs to the rate of insulin release, will be

determined by type of diabetes, age, sex, weight, height, body fat ratio and some other parameters. With this initial transition function, the patch will be able to work properly. By anticipate the glucose level and compare it the real value, the system can also calibrate itself through the use. Thus give more accurate personal data through time.
With input and the transition function, we should get a blood glucose level which is monitored by the sensor. The data from the sensor will affect the release rate and keep the glucose level in a desired range.

2.Inverse piezoelectric control mechanism

Piezoelectric effect was first discovered in 1880 by Jacques and Pierre Curie **[34]**. When a mechanical stress or pressure is added on a piezoelectric material, there will be charge cumulate on each side. Correspondingly an inverse piezoelectric effect would be when voltage is added on material, it will either stretch or shrink depend on whether the voltage is positive or negative. Our proposal here is to take advantage of this effect to control the release rate of the drug.

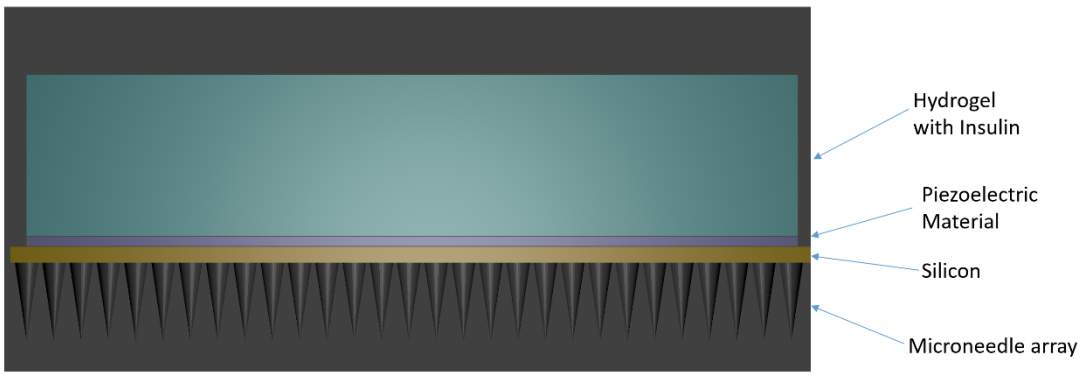

Fig.2 Side view of microneedle array, piezoelectric controller and hydrogel

As shown in **Fig. 2**, the piezoelectric control part will lay between the hydrogel and the microneedle array. They have holes corresponding to the place of the microneedles. So the insulin within the hydrogel can get into human body by diffusion. By lifting the hydrogel up or down, we can control the diffusion rate of the drug.

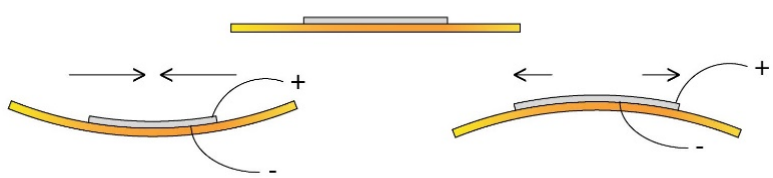

Fig.3 Diagram shows two different curve direction on the piezoelectric controller

As shown in **Fig. 3**, the top part is piezoelectric material, the bottom part is silicon. These two layers are bonded together. When no voltage is added, two thin parts are flat and the hydrogel will diffuse the drug through the needle to the blood vessel. When voltage applied, the upper layer will shrink or extend, since they are bonded together, this will curve the plane. In the left situation, the release rate will be reduced, and in the right situation, the release of the drug will be terminated. The lifted distance will be within 500μm. Hence the user will not notice the difference. Thus the release of drug will be slowed since the drug delivery method is based on diffusion.

3. Integration of the system and soft electronics fabrication

Everything is integrated in a single patch. The whole system includes the following components (i)

the microneedle array, (ii) the piezoelectric controller, (iii) the insulin hydrogel, (iv) the battery, (v) the sweat glucose sensor, (vi) radio frequency data transporter and (vii) microchip set for data processing. To integrate these functions onto the skin, our proposal is to make a soft microfluidic assembly of these components. This idea was inspired by Xu et al. **[29]**, but with some modification.

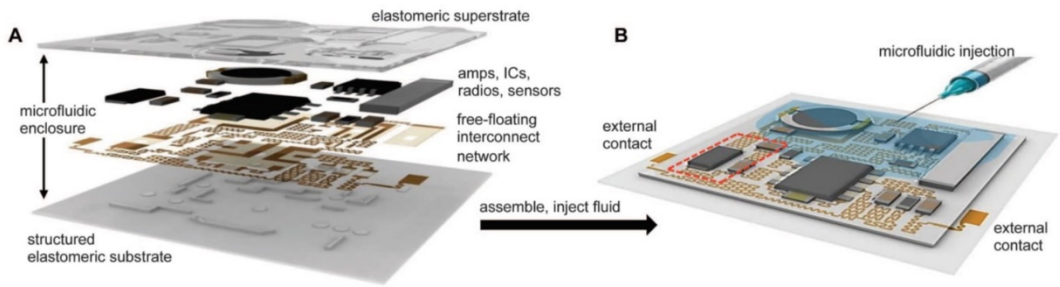

Fig.4 A demonstration of how the integration of soft electronics is done **[29]**

The idea here is to use silicone elastic materials (Ecoflex) to build a substrate and superstrate, encapsulate all the components into this microfluidic device. Every component was bounded to a certain place in the whole device by support post. These support post will isolate the deformation of the substrate from the components. All the components are immersed in liquid, further insolated them with the substrate.

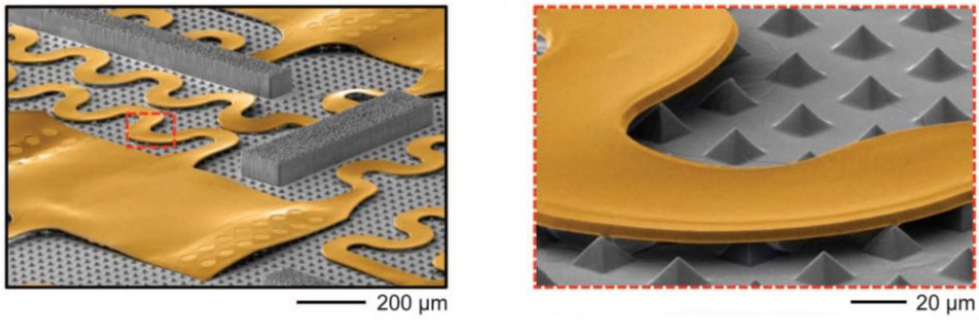

Fig.5 A demonstration of how the pyramid lift up the wires and give extra degree of freedom **[29]**

The components are connected by free floating wires. These wires will also be attached to the substrate at some point by the support post, usually the same support post for corresponding component. The free floating part were made spring like to ensure good elasticity. The material of these wires should be flexible and antifatigue. As shown in picture, when these wires are unstretched they are in the same plane in 2D. When stretched to certain length, they will bend and twist. Hence become 3D. Thar is why on the substrate there are periodic small pyramid embossment. The wires will be deposit on these pyramid and the space lifted by them is for extra degree of freedom, so the deformation of the wire will not be constrained. Additional to this, the whole device is filled with fluid for more smooth stretching and deformation.

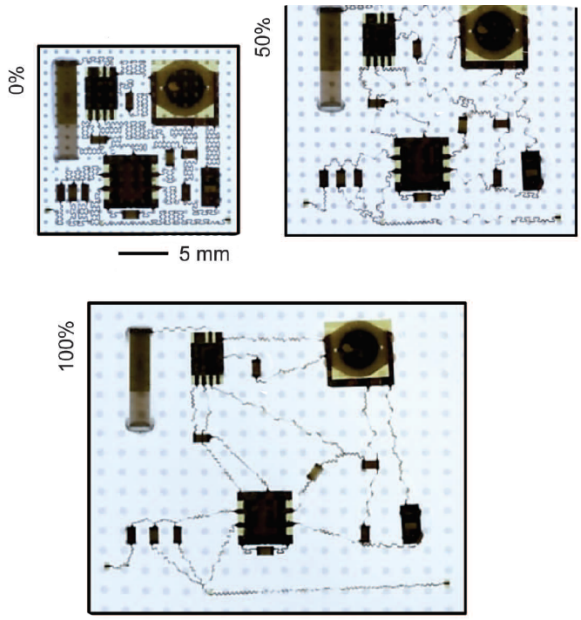

Fig.6 A demonstration of how the substrate stretch and all the wire remain connected **[29]**

The fluid itself needs to meet many criteria **[29]**. In short, it should have high volume resistivity and high dielectric strength so that the electric components can work separately without any interruption. It should have good thermal stability and non-biohazard to work closely with human body. Ideally it should be transparent through the visible light spectrum to radio frequency, to eliminate the affect for data transition and easy to inspect the component inside. The fluid chosen here is a high molecular weight silicone oligomer.

In our proposal, there are two components should be directly against the skin. The microneedle array and the sweat glucose sensor. First of all, we will make the microneedle array, the piezoelectric controller and the hydrogel into a single capsulation, we will call this drug box. The silicone elastomer make substrate will be deposit onto the drug box and the sweat sensor. The sensor and drug box will have glue on top to make firm attach to the substrate. Then deposit the wire and other components on the substrate. The wire is connected to sensor and drug box at right contactor. Close the patch by superstrate and inject fluid to finalize the manufacture process.

V. References

[1] Kim, Y.-C., Park, J.-H., and Prausnitz, M. R. "**Microneedles For Drug and Vaccine Delivery**" *Advanced Drug Delivery Reviews* 64, no. 14 (2012): 1547–1568. doi:10.1016/j.addr.2012.04.005,

[2] Pegoraro, C., Macneil, S., and Battaglia, G. "**Transdermal Drug Delivery: from Micro to Nano**" *Nanoscale* 4, no. 6 (2012): 1881. doi:10.1039/c2nr11606e,

[3] Mukerjee, E., Collins, S., Isseroff, R., and Smith, R. "**Microneedle Array for Transdermal Biological Fluid Extraction and in Situ Analysis**" *Sensors and Actuators A: Physical* 114, no. 2-3 (2004): 267–275. doi:10.1016/j.sna.2003.11.008,

[4] Ma, B., Liu, S., Gan, Z., Liu, G., Cai, X., Zhang, H., and Yang, Z. "**A PZT Insulin Pump Integrated With a Silicon Micro Needle Array for Transdermal Drug Delivery**" *56th Electronic Components and Technology Conference 2006* doi:10.1109/ectc.2006.1645724,

[5] C., Kumar, A., C., Li, X., Sandoval, M. A., Rodriguez, L. B., and Sloat, B. R. "**Permeation Of Antigen Protein-Conjugated Nanoparticles and Live Bacteria through Microneedle-Treated Mouse Skin**" *International Journal of Nanomedicine IJN* (2011): 1253. doi:10.2147/ijn.s20413,

[6] Donnelly, R. F., Singh, T. R. R., Tunney, M. M., Morrow, D. I. J., Mccarron, P. A., O'Mahony, C., and Woolfson, A. D. "**Microneedle Arrays Allow Lower Microbial Penetration Than Hypodermic Needles In Vitro**" *Pharm Res Pharmaceutical Research* 26, no. 11 (2009): 2513–2522. doi:10.1007/s11095-009-9967-2,

[7] Gupta, J., Gill, H. S., Andrews, S. N., and Prausnitz, M. R. "**Kinetics Of Skin Resealing after Insertion of Microneedles in Human Subjects**" *Journal of Controlled Release* 154, no. 2 (2011): 148–155. doi:10.1016/j.jconrel.2011.05.021,

[8] Xu, Z. "**Nanoreplicated Positive and Inverted Submicrometer Polymer Pyramid Array for Surface-Enhanced Raman Spectroscopy**" *Journal of Nanophotonics J. Nanophoton* 5, no. 1 (2011): 053526. doi:10.1117/1.3663259,

[9] Archer, M. J. and Ligler, F. S. "**Fabrication And Characterization of Silicon Micro-Funnels and Tapered Micro-Channels for Stochastic Sensing Applications**" *Sensors* 8, no. 6 (2008): 3848–3872. doi:10.3390/s8063848,

[10] Williams, K., Gupta, K., and Wasilik, M. "**Etch Rates for Micromachining Processing-Part II**" *Journal of Microelectromechanical Systems J. Microelectromech. Syst.* 12, no. 6 (2003): 761–778. doi:10.1109/jmems.2003.820936,

[11] Hosseinnia, A. H., Atabaki, A. H., Eftekhar, A. A., and Adibi, A. "**High-Quality Silicon on Silicon Nitride Integrated Optical Platform with an Octave-Spanning Adiabatic Interlayer Coupler**" *Opt. Express Optics Express* 23, no. 23 (2015): 30297. doi:10.1364/oe.23.030297,

[12] Kastenmeier, B. E. E., Matsuo, P. J., and Oehrlein, G. S. "**Highly Selective Etching of Silicon Nitride over Silicon and Silicon Dioxide**" *Journal of Vacuum Science & Technology A: Vacuum, Surfaces, and Films J. Vac. Sci. Technol. A* 17, no. 6 (1999): 3179. doi:10.1116/1.582097,

[13] Lee, H., Choi, T. K., Lee, Y. B., Cho, H. R., Ghaffari, R., Wang, L., Choi, H. J., Chung, T. D., Lu, N., Hyeon, T., Choi, S. H., and Kim, D.-H. "**A Graphene-Based Electrochemical Device with Thermoresponsive Microneedles for Diabetes Monitoring and Therapy**" *Nature Nanotech Nature Nanotechnology* (2016): doi:10.1038/nnano.2016.38,

[14] Xu, L., Gutbrod, S. R., Bonifas, A. P., Su, Y., Sulkin, M. S., Lu, N., Chung, H.-J., Jang, K.-I., Liu, Z., Ying, M., Lu, C., Webb, R. C., Kim, J.-S., Laughner, J. I., Cheng, H., Liu, Y., Ameen, A., Jeong, J.-W., Kim, G.-T., Huang, Y., Efimov, I. R., and Rogers, J. A. "**3D Multifunctional**

Integumentary Membranes for Spatiotemporal Cardiac Measurements and Stimulation across the Entire Epicardium" *Nature Communications Nat Comms* 5, (2014): doi:10.1038/ncomms4329,

[15] Guinovart, T., Bandodkar, A. J., Windmiller, J. R., Andrade, F. J., and Wang, J. "**A Potentiometric Tattoo Sensor for Monitoring Ammonium in Sweat**" *The Analyst Analyst* 138, no. 22 (2013): 7031. doi:10.1039/c3an01672b,

[16] Jia, W., Bandodkar, A. J., Valdés-Ramírez, G., Windmiller, J. R., Yang, Z., Ramírez, J., Chan, G., and Wang, J. "**Electrochemical Tattoo Biosensors For Real-Time Noninvasive Lactate Monitoring in Human Perspiration**" *Analytical Chemistry Anal. Chem.* 85, no. 14 (2013): 6553–6560. doi:10.1021/ac401573r,

[17] Bandodkar, A. J., Jia, W., Yardımcı, C., Wang, X., Ramirez, J., and Wang, J. "**Tattoo-Based Noninvasive Glucose Monitoring: A Proof-Of-Concept Study**" *Analytical Chemistry Anal. Chem.* 87, no. 1 (2015): 394–398. doi:10.1021/ac504300n,

[18] Olarte, O., Chilo, J., Pelegri-Sebastia, J., Barbe, K., and Moer, W. V. "**Glucose Detection in Human Sweat Using an Electronic Nose**" *2013 35th Annual International Conference of the IEEE Engineering in Medicine and Biology Society (EMBC)* (2013): doi:10.1109/embc.2013.6609787,

[19] Kost, J., Mitragotri, S., Gabbay, R. A., Pishko, M., and Langer, R. "**Transdermal Monitoring of Glucose and Other Analytes Using Ultrasound**" *Nature Medicine* 6, (2000): 347–350. doi:10.1038/73213,

[20] Ahmed, E. M. "**Hydrogel: Preparation, Characterization, and Applications: A Review**" *Journal of Advanced Research* 6, no. 2 (2015): 105–121. doi:10.1016/j.jare.2013.07.006,

[21] Darnell, M. C., Sun, J.-Y., Mehta, M., Johnson, C., Arany, P. R., Suo, Z., and Mooney, D. J. "**Performance And Biocompatibility of Extremely Tough Alginate/Polyacrylamide Hydrogels**" *Biomaterials* 34, no. 33 (2013): 8042–8048. doi:10.1016/j.biomaterials.2013.06.061,

[22] Yim, E. S., Zhao, B., Myung, D., Kourtis, L. C., Frank, C. W., Carter, D., Smith, R. L., and Goodman, S. B. "**Biocompatibility Of Poly(Ethylene Glycol)/Poly(Acrylic Acid) Interpenetrating Polymer Network Hydrogel Particles in RAW 264.7 Macrophage and MG-63 Osteoblast Cell Lines**" *Journal of Biomedical Materials Research Part A J. Biomed. Mater. Res.* 91A, no. 3 (2009): 894–902. doi:10.1002/jbm.a.32311,

[23] Qiu, Y. and Park, K. "**Environment-Sensitive Hydrogels for Drug Delivery**" *Advanced Drug Delivery Reviews* 53, no. 3 (2001): 321–339. doi:10.1016/s0169-409x(01)00203-4,

[24] Saxena, V. "**Temperature Distribution in Human Skin and Subdermal Tissues**" *Journal of Theoretical Biology* 102, no. 2 (1983): 277–286. doi:10.1016/0022-5193(83)90365-x,

[25] Cha, R., He, Z., and Ni, Y. "**Preparation And Characterization of Thermal/PH-Sensitive Hydrogel from Carboxylated Nanocrystalline Cellulose**" *Carbohydrate Polymers* 88, no. 2 (2012): 713–718. doi:10.1016/j.carbpol.2012.01.026,

[26] Tu, H., Heitzman, C. E., and Braun, P. V. "**Patterned Poly(N -Isopropylacrylamide) Brushes on Silica Surfaces by Microcontact Printing Followed by Surface-Initiated Polymerization**" *Langmuir* 20, no. 19 (2004): 8313–8320. doi:10.1021/la049663a,

[27] Alcantar, N. A., Aydil, E. S., and Israelachvili, J. N. "**Polyethylene Glycol-Coated Biocompatible Surfaces**" *Journal of Biomedical Materials Research J. Biomed. Mater. Res.* 51, no. 3 (2000): 343–351. doi:10.1002/1097-4636(20000905)51:3<343::aid-jbm7>3.0.co;2-d,

[28] Khetan, S. and Burdick, J. A. "**Patterning Hydrogels in Three Dimensions towards Controlling Cellular Interactions**" *Soft Matter* 7, no. 3 (2011): 830–838. doi:10.1039/c0sm00852d,

[29] Xu, S., Zhang, Y., Jia, L., Mathewson, K. E., Jang, K.-I., Kim, J., Fu, H., Huang, X., Chava, P., Wang, R., Bhole, S., Wang, L., Na, Y. J., Guan, Y., Flavin, M., Han, Z., Huang, Y., and Rogers,

J. A. "**Soft Microfluidic Assemblies Of Sensors, Circuits, and Radios for the Skin**" *Science* 344, no. 6179 (2014): 70–74. doi:10.1126/science.1250169,

[30] Xu, S., Zhang, Y., Cho, J., Lee, J., Huang, X., Jia, L., Fan, J. A., Su, Y., Su, J., Zhang, H., Cheng, H., Lu, B., Yu, C., Chuang, C., Kim, T.-I., Song, T., Shigeta, K., Kang, S., Dagdeviren, C., Petrov, I., Braun, P. V., Huang, Y., Paik, U., and Rogers, J. A. "**Stretchable Batteries with Self-Similar Serpentine Interconnects and Integrated Wireless Recharging Systems**" *Nature Communications Nat Comms* 4, (2013): 1543. doi:10.1038/ncomms2553,

[31] Han, F., Meng, G., Zhou, F., Song, L., Li, X., Hu, X., Zhu, X., Wu, B., and Wei, B. "**Dielectric Capacitors with Three-Dimensional Nanoscale Interdigital Electrodes for Energy Storage**" *Science Advances* 1, no. 9 (2015): doi:10.1126/sciadv.1500605,

[32] Fan, J. A., Yeo, W.-H., Su, Y., Hattori, Y., Lee, W., Jung, S.-Y., Zhang, Y., Liu, Z., Cheng, H., Falgout, L., Bajema, M., Coleman, T., Gregoire, D., Larsen, R. J., Huang, Y., and Rogers, J. A. "**Fractal Design Concepts for Stretchable Electronics**" *Nature Communications Nat Comms* 5, (2014): doi:10.1038/ncomms4266,

[33] "**IDF Diabetes Atlas - 7th Edition**" *IDF diabetes atlas* Available at http://www.diabetesatlas.org/

[34] Manbachi, A. and Cobbold, R. S. C. "**Development And Application of Piezoelectric Materials for Ultrasound Generation and Detection**" *Ultrasound* 19, no. 4 (2011): 187–196. doi:10.1258/ult.2011.011027,

VI. Budget proposal

ECE 481 Budget Template							
4 year draft budget							
Category	**Appt Type**	**Salary**	**Year 1**	**Year 2**	**Year 3**	**Year 4**	**4-Year Total**
Personnel:							
Professor 1	1 summer month	100,000	11,111	11,444	11,787	12,141	46,483
2 Graduate Students	12 Months @100%	48,000	5,333	5,493	5,658	5,941	22,425
3 Undergraduate Students	8 Months @50%	15,840	1,760	1,813	1,867	1,960	7,400
			0	0	0	0	0
			0	0	0	0	0
			0	0	0	0	0
							0
Fringe			4,875	5,021	5,172	5,367	20,435
							0
Total Salaries, Wages & Fringe			23,079	23,771	24,484	25,409	96,743
							0
Equipment			20,000	10,000	5,000	5,000	40,000
Cleanroom Access	12 Months @100%	180,000	180,000	180,000	180,000	180,000	720,000
							0
							0
Travel							0
Domestic:			5,000	5,000	5,000	5,000	20,000
							0
							0
Other Direct Costs:							0
Materials and Supplies			15,000	15,450	15,914	16,391	62,754
Publication Costs			5,000	5,150	5,305	5,464	20,918
Tuition Remission 34.5%			0	0	0	0	0
							0
							0
Total Direct Costs			248,079	239,371	235,702	237,264	960,416
Indirect Costs (Overhead)							
MTDC 53%			120,882	121,567	122,272	123,100	487,821
Total Overhead			120,882	121,567	122,272	123,100	487,821
							0
Total Costs			368,961	360,938	357,974	360,364	1,448,237